Iran Polym J (2017) 26:811–819
DOI 10.1007/s13726-017-0561-x

ORIGINAL PAPER

Biodegradable poly(vinyl alcohol)-based nanocomposite film reinforced with organophilic layered double hydroxides with potential packaging application

Jiazhuo Xie[1,2] · Kun Zhang[1] · Zhou Wang[3] · Qinghua Zhao[4] · Yuechao Yang[2] · Yanfei Zhang[1] · Shiyun Ai[1] · Jing Xu[1]

Received: 27 February 2017 / Accepted: 29 August 2017 / Published online: 27 October 2017

Abstract The continuously increasing plastic wastes and diminishing fossil resources have attracted global attention into research and development of biodegradable packaging materials. In the present study, organophilic layered double hydroxides (OLDH) intercalated with aliphatic long-chain molecules as reinforcing agents were incorporated into biodegradable poly(vinyl alcohol) (PVA) matrix by a solution casting method. FTIR, XRD and SEM were performed to analyze the structure of PVA/OLDH films. The OLDH nanosheets were well-dispersed in PVA matrix and formed strong interfacial interactions with the PVA chains, leading to remarkable improvements of optical property, mechanical performance, water vapor barrier property and thermal stability. At a loading of only 2% OLDH in PVA, we observed ~67% decrease in haze and ~66% increment in tensile strength in the composite film compared with pure PVA film. Furthermore, a 24.22% decrease in water vapor permeability (enhancement in water vapor barrier property) due to the addition of 0.5 wt% OLDH and enhanced thermal stability could be observed. These results revealed that the overall performance could be improved by introducing OLDH at very low loadings and that the PVA nanocomposite films have potential for future application in packaging films. Therefore, the use of high-performance PVA/OLDH nanocomposite films can evidently promote the application of biodegradable PVA materials in packaging industry.

Keywords Packaging application · Biodegradable nanocomposite films · Poly(vinyl alcohol) · Organophilic layered double hydroxides · Enhanced properties

✉ Shiyun Ai
ashy@sdau.edu.cn

✉ Jing Xu
jiaxu@sdau.edu.cn

[1] College of Chemistry and Material Science, Shandong Agricultural University, Tai′an 271018, People's Republic of China

[2] National Engineering Laboratory for Efficient Utilization of Soil and Fertilizer Resources, National Engineering and Technology Research Center for Slow and Controlled Release Fertilizers, College of Resources and Environment, Shandong Agricultural University, Tai′an 271018, People's Republic of China

[3] National Engineering Technology Research Center for SCRF, Kingenta Ecological Engineering Group Co., Ltd, Linshu 276700, People's Republic of China

[4] Department of Basic Courses, Shandong Medicine Technician College, Tai′an 271000, People's Republic of China

Introduction

Over the past few decades, due to increased awareness on the continuously increasing plastic wastes and decreasing fossil resources, the potential application of eco-friendly polymers as biodegradable packaging materials has attracted steadily ever-increasing attentions worldwide [1–3]. Recently, poly(butylene adipate-*co*-terephthalate), poly(propylene carbonate), polylactide, poly(vinyl alcohol) and their biodegradable derivatives have been widely investigated to replace the non-biodegradable petrochemical-based counterparts [4–6]. Among the well-recognized biodegradable polymers, poly(vinyl alcohol) (PVA) is a completely biodegradable polymer, which can be eventually degraded into carbon dioxide and water with selective bacteria in soil. Moreover, PVA as a non-toxic and non-carcinogenic polymer with extraordinary film formation characteristic, good chemical resistance and anti-electrostatic properties is considered as one of the most promising biodegradable

packaging film materials [7–9]. However, the poor mechanical, optical and water vapor barrier properties of PVA have restricted its wide application in packaging materials. To solve these problems, one of the most effective ways is to blend PVA with other materials (e.g., nanoparticles) in low volume to fabricate nanocomposite films with enhanced properties, while its biodegradability characteristics remain unchanged [10, 11]. Recently, some works have been made to improve the individual properties of PVA films, such as optical properties, mechanical performances and water barrier properties, respectively [12–14]. Nevertheless, there are rare reports on the effects of reinforcements on the overall performance of PVA nanocomposites, which are exactly selected in their applications as textile, pesticide, and electronic product packaging materials.

Layered double hydroxides (LDHs) are a class of inorganic layered clays which can be given a specific function by changing the chemical composition of positively charged metal layer and the anion in the interlayer space [15–17]. To achieve a homogeneous dispersion of LDH particles into a biodegradable polymer matrix, research efforts were focused on obtaining organophilic layered double hydroxides (OLDHs) by introducing diverse organic anion [18–20]. LDH and OLDH have been widely used as reinforcement agents in polymer matrices for enhanced mechanical and water barrier properties [21–23]. Zhou et al. introduced LDH nanoplates into PVA matrix as reinforcing agents to improve the fire resistance and mechanical properties of PVA film [24]. Marangoni et al. prepared a composite of PVA and OLDH (intercalated with orange dyes) by solution casting process, which improved the Young's modulus distinctly [25]. In our previous work, OLDH was synthesized by facile introduction of aliphatic long-chain molecules into the interlayers, and we found the organo-modified LDH nanosheets could overcome the hydrogen bond attraction between the lamellae and easily exfoliate and disperse well in the biopolymer matrix. Meanwhile, as far as we know, the layered double hydroxides, with refractive indices similar to those of most polymers, provide a distinct advantage as fillers in the transparent polymer packaging films. All the above aspects have inspired us to fabricate the biodegradable PVA/OLDH nanocomposite films to achieve optical, mechanical and water vapor barrier properties to expand the application of PVA material in the packaging field.

In this work, PVA/OLDH nanocomposite films with low OLDH content were successfully fabricated by solution casting method. The OLDH was prepared by introducing an aliphatic long-chain molecule into the interlayer of LDH to impart better compatibility with PVA matrix [26]. The effects of OLDH content on the morphologies and properties (e.g., optical, mechanical, water vapor barrier properties and thermal stability) of PVA-based nanocomposite films were also studied.

Experimental

Materials

Al $(NO_3)_3 \cdot 9H_2O$ (99%), $Zn(NO_3)_2 \cdot 6H_2O$ (99%), NaOH (99%), HNO_3 (65.0–68.0%) and potassium dodecyl phosphate (PDP) (97%) were purchased from Aladdin Reagent Co., Ltd. (Shanghai, China). Poly(vinyl alcohol) (PVA) with average degree of polymerization of 1750 ± 50 was supplied by BASF Chemical Co., Ltd. (Tianjin, China). Deionized water was distilled before use to remove the carbon dioxide dissolved in water. All reagents were analytical grade and used as received.

Preparation of OLDH

The OLDH powder was prepared by anion-exchange method. First, the LDH precursor was synthesized by a method involving separated nucleation and aging steps [27]. Then, 5.0 g of LDH precursor and 30 mL of PDP were added into a three-necked, round-bottomed flask. The pH of mixture was adjusted to 4.5 by dropwise addition of HNO_3. After ultrasonic concussion for 30 min, the white slurry was aged with vigorous stirring at 100 °C under nitrogen atmosphere for 48 h. The precipitate was filtered and washed three times with deionized water. Finally, the white OLDH product was obtained after being dried at 70 °C for 24 h.

Fabrication of PVA/OLDH films

The PVA/OLDH films were fabricated by solution casting method. First, an adequate amount of OLDH powder and 30 mL of deionized water were added into a 100 mL three-necked, round-bottomed flask. After ultrasonic concussion for 20 min, a given amount of PVA powder was subsequently dispersed into the obtained OLDH slurry. Then, the mixture was stirred vigorously at reflux temperature under nitrogen atmosphere for 3 h to obtain a homogeneous aqueous solution. Finally, the PVA/OLDH solution was poured onto a surface of glass plate (15 cm × 15 cm × 3 cm). After being placed under air atmosphere for 12 h, the obtained PVA/OLDH films were treated at 50 °C for another 12 h to remove the residual moisture. The thickness of the PVA/OLDH films was 75 ± 5 μm. The mass ratios of PVA and OLDH were 100/0, 99.5/0.5, 99/1, 98/2, 97/3 and 96/4, respectively, designated as OLDH-0, OLDH-0.5, OLDH-1, OLDH-2, OLDH-3 and LDH-4 accordingly. The fabrication process steps of PVA/OLDH films are shown in Fig. 1, respectively.

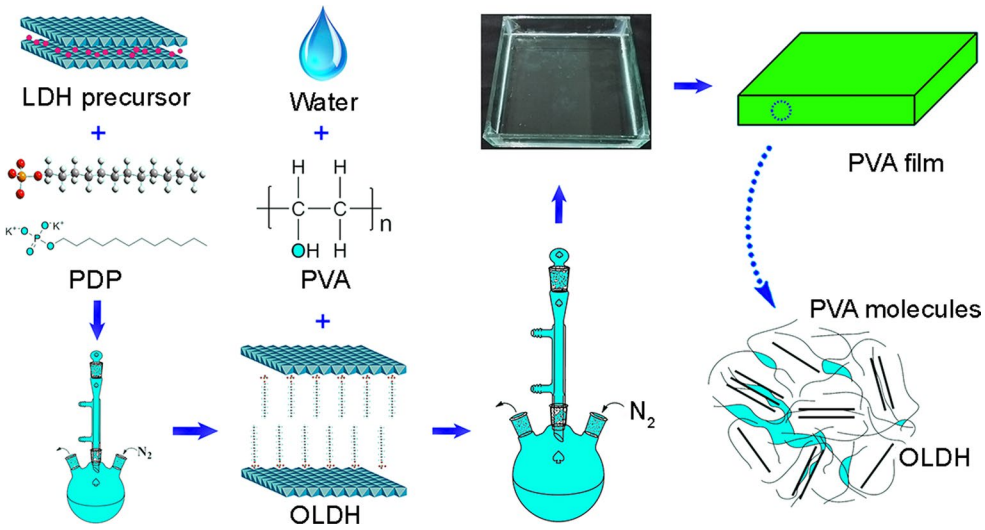

Fig. 1 Schematic diagram for fabrication process of PVA/OLDH films

Structural analysis

The FTIR spectra were recorded using KBr pellet on a Nicolet 380 Fourier transform infrared spectrometer (Thermo, America) with a resolution of 4 cm^{-1} from 4000 to 400 cm^{-1}. The XRD patterns were collected by an X-ray single crystal diffractometer (D8 Quest, Bruker, Germany) in the range of $2\theta = 1.5°–50°$ with a voltage of 40 kV and tube current of 40 mA using CuKα radiation ($\lambda = 1.54056$ Å) at room temperature. The morphologies of the fracture surface of PVA/OLDH films were studied by a scanning electron microscope (Jeol 6400F, Japan Electron Optics Ltd., Japan) at 20 kV after being coated with gold.

Performance studies

The visible light transmittance and haze were obtained with a light transmittance/haze tester (WGT-2S, Yidian Physical Optical Instrument Co., Ltd., China) in accordance with national standard GB 2410-2008. Each specimen was measured three times to obtain the average value. The nominal tensile strain-at-break and tensile strength were measured by an electronic universal testing machine (UTM2502, Suns Technology Stock Co., Ltd., China) using dumbbell-shaped specimens according to GB/T1040.3-2006 standard with a speed of 200 mm min^{-1}. Each sample was measured five times to obtain the average value. The water vapor permeability (WVP) was measured by an automatic water vapor transmission tester (PERME W3/030, Instrument Technology Co., Ltd., China) using round specimens (diameter: 0.074 m; area: 3.3×10^{-3} m^2) according to GB1037-88 standard. The WVP values were calculated according to Eq. (1) as follows:

$$\mathrm{WVP}(\mathrm{g} \times \mathrm{cm}/\mathrm{cm}^2 \times \mathrm{s} \times \mathrm{Pa}) = (\Delta m \times d)/(A \times t \times \Delta P), \quad (1)$$

where, Δm (g) is the mass loss of water vapor passing through the specimen; d (cm) is the thickness of the specimen; A (cm^2) is the area of the specimen; t (s) is the measured time interval; ΔP (Pa) is the water vapor pressure difference on both sides of the specimen.

The thermogravimetric analysis (TGA) and derivative thermogravimetry (DTG) curves were recorded using an automatic thermal analysis instrument (DTG-60 A, Shimadzu, Japan) from 30 to 600 °C at a heating rate of 10 °C min^{-1} under nitrogen atmosphere with 5–10 mg sample mass.

Results and discussion

Structural characterization

The FTIR absorption spectra of OLDH powder, OLDH-0 and OLDH-4 are shown in Fig. 2. For OLDH powder (Fig. 2a), the absorption bands at 3437 and 1635 cm^{-1} are related to the –OH stretching and bending vibrations between the OLDH layers, respectively, while the absorption peak at 587 cm^{-1} is assigned to the bending vibration of the metal–oxygen bonds in the OLDH layers [28, 29]. It is worth mentioning that, the C–H stretching and scissoring vibrations at 2928, 2847 and 1466 cm^{-1} [30], and the stretching vibration of P–O groups at 1089 cm^{-1} are related to PDP molecules, revealing the successful formation of OLDH phase.

For PVA films (Fig. 2b, c), the absorption peaks at 3437 and 1635 cm^{-1} can be attributed to the –OH groups of water in the films, while the C–H scissoring vibration of PVA molecule is observed at 1409 cm^{-1}. The differences in the FTIR spectra of OLDH-0 and OLDH-4 are noticeable. The newly emerging characteristic peaks of C–H stretching and P–O

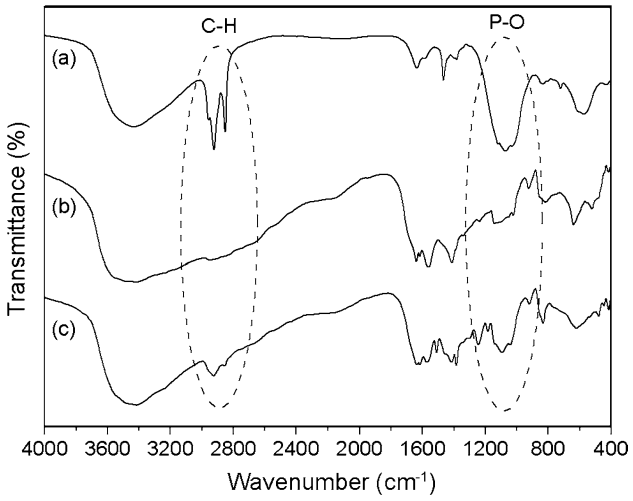

Fig. 2 FTIR spectra of **a** OLDH powder; **b** OLDH-0; and **c** OLDH-4

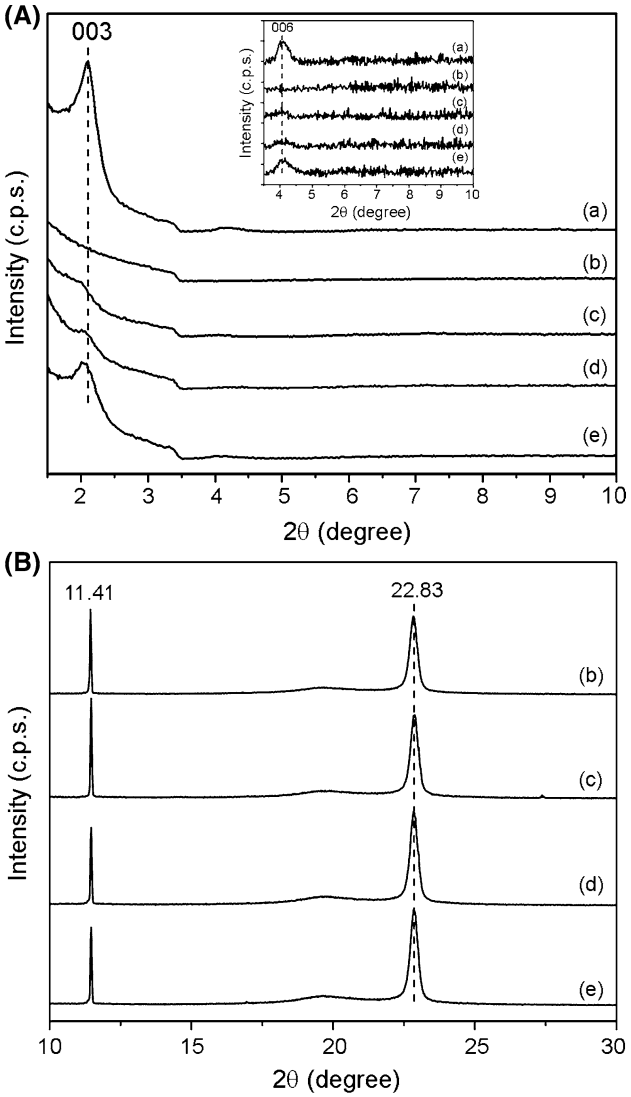

Fig. 3 **A** XRD patterns of *a* OLDH powder; *b* OLDH-0; *c* OLDH-1; *d* OLDH-2; and *e* OLDH-4 in the angle of $2\theta = 1.5°–10°$, **B** XRD patterns of *a* OLDH-0; *b* OLDH-1; *c* OLDH-2; and *d* OLDH-4 in the range of $2\theta = 10°–50°$

stretching vibrations observed at 2928, 2847 and 1089 cm^{-1} demonstrate the successful incorporation of OLDH nanoparticles into the PVA matrix.

The XRD patterns of the OLDH powder, OLDH-0, OLDH-1, OLDH-2 and OLDH-4 samples are displayed in Fig. 3. For OLDH powder in Fig. 3A(a), the Bragg reflections (003) and (006) at $2\theta = 2.10°$ and 4.06° reveal the well-developed layer structure of OLDH [31]. There are apparent differences between the PVA films shown in Fig. 3A (b–e). In the lower concentration range (1%), there is no evidence of crystalline phases from the OLDH used as filler. However, at 2%, such diffraction peaks start to be observed, and at 4% filler concentration, a broad peak can be clearly observed. A small increase of 0.1 Å in the basal distance of the original intercalated materials is observed for OLDH-2 and OLDH-4 samples, respectively, which most likely indicates partial co-intercalation of PVA. This effect certainly contributes to the homogeneity of the obtained films [25]. Furthermore, as Fig. 3B(b–d) shows, there are no changes in the reflection peaks of the OLDH-0, OLDH-1, OLDH-2 and OLDH-4 samples at $2\theta = 11.41°$, 22.83°, 34.55° and 48.25°, revealing that the incorporation of nanosized OLDH has no significant influence on the crystalline structure of PVA matrix [26].

Morphology of fracture surfaces

The microstructures of the fractured surfaces of neat PVA and PVA/OLDH films were studied using SEM. The images of sample films (OLDH-0, OLDH-0.5, OLDH-1, OLDH-2, OLDH-3 and OLDH-4) at two resolutions are shown in Fig. 4. As can be seen in Fig. 4a, A, the morphology of neat PVA film is quite smooth. In contrast, the roughness of fracture surface of PVA/OLDH films increases with increasing OLDH loading (0.5, 1, 2 and 3%) as, respectively, shown in Fig. 4b–e, suggesting a well dispersion of OLDH in the matrix and the formation of strong interfacial interactions. However, as it is evident in Fig. 4f, F, the partial surface morphology again reveals a rather smooth surface with further increase in OLDH content up to 4%, which can be attributed to the presence of aggregated OLDH particles probably due to insufficient dispersion of the OLDH nanosheets at high concentration. In other words, only the well-exfoliated OLDH nanosheets can form the hydrogen bonding networks with the PVA chains effectively, and can improve the dispersibility of OLDH in the PVA matrix. The good dispersion and strong interfacial interactions contributed by low OLDH loading are predictable for improved properties discussed in later sections.

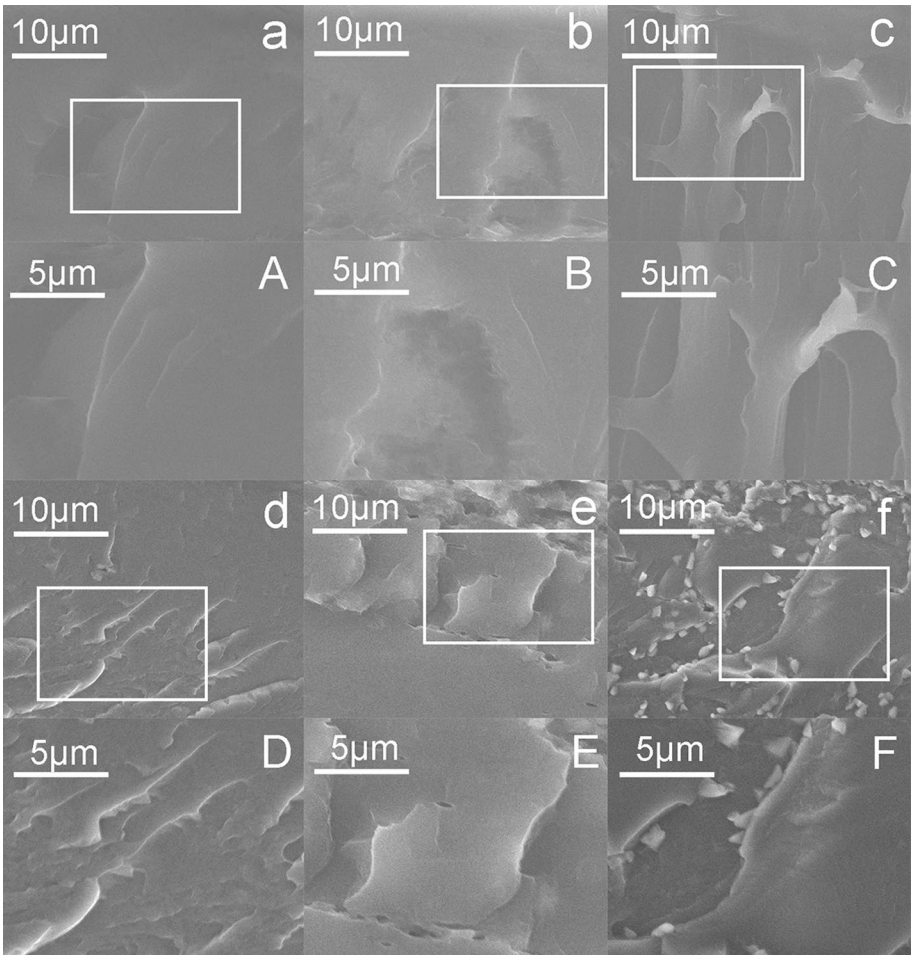

Fig. 4 SEM micrographs of fracture surfaces of **a**, **A** OLDH-0, **b**, **B** OLDH-0.5, **c**, **C** OLDH-1, **d**, **D** OLDH-2, **e**, **E** OLDH-3, and **f**, **F** OLDH-4. **a**–**f** and **A**–**F** images were magnified ×2000 and ×4000, respectively

Optical properties

The visible light transmittance and haze curves of OLDH-0, OLDH-0.5, OLDH-1, OLDH-2, OLDH-3 and OLDH-4 are displayed in Fig. 5. As seen, the optical properties of PVA/OLDH films are closely related to the OLDH loading. The visible light transmittance increases at first and then decreases with the increase in OLDH loading, indicating the aggregation of smaller OLDH particles into larger size particles at high loading.

The reduced haze is attributed to the similar refraction coefficients of OLDH powder (1.50) and PVA matrix (1.49–1.53). The optimal optical performance was found to be that of the film of OLDH-2 with a 66.97% decrease in haze value (17.18%) and a 5.92% enhancement in visible light transmittance value (92.78%). The significant improvement in optical properties could be attributed to the effect of heterogeneous nucleation induced by the nanosized OLDH particles in the PVA matrix, which was similarly observed in previous published works [4, 32]. Heterogeneous nucleation is a crystallization process in which the PVA chains can be adsorbed on the interfaces of nanosized OLDH particles

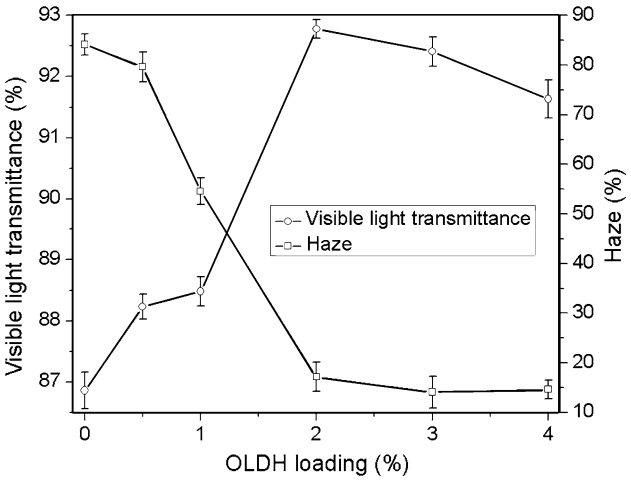

Fig. 5 Visible light transmittance and haze variations as functions of OLDH loading

to form tiny crystals with homogeneous size distribution, which, in turn, can reduce the light refraction between the PVA matrix and external environment to improve the optical

properties of PVA/OLDH films compared with a neat PVA film. Furthermore, a uniform and fine nanosized distribution of OLDH particles can also be confirmed by SEM images shown in Fig. 4. In fact the enhanced transparency will be obtained if the size of individual nanoparticles is smaller than the visible light wavelength [33].

Mechanical performance

The influence of OLDH loading on mechanical performance (nominal tensile strain-at-break and tensile strength) of PVA/OLDH films is shown in Fig. 6. The mechanical performance of neat PVA film is also given in this figure. The nominal tensile strain-at-break and tensile strength show rising trends at low OLDH content range and decreasing trends at high loading range. In comparison with pure PVA film, the values of nominal tensile strain-at-break and tensile strength with 35.15 and 65.97% improvements were found to be 952.05% and 47.02 MPa, respectively. The significant improvements can be attributed in good exfoliation and uniform dispersion of nanosized OLDH particles, resulting in vast nanometric junctions to enhance the combination of nanoparticles with that of PVA matrix. In addition, the long-chain plasticizer in OLDH interlayers promotes the interfacial bonds between the OLDH and PVA matrix [4, 34].

The tensile strength value and the change in the performance with increasing the OLDH content obtained for PVA/OLDH film were the same as those reported in Ref. [35]. However, different results were obtained with the nominal tensile strain-at-break values, which could be attributed to a significant difference between the average molecular weights. Furthermore, the PVA/OLDH (2%) film revealed the optimal mechanical performance both in our work and the previous results reported earlier [35].

Water vapor barrier properties

The water vapor barrier property (WVP) measurements carried out on pure PVA film (OLDH-0) and PVA/OLDH films (OLDH-0.5, OLDH-1, OLDH-2, OLDH-3 and OLDH-4) are shown in Fig. 7. As seen, the WVP of the PVA films is improved by adding the nanosized OLDH particles at low content. The OLDH-0.5 shows the best WVP value corresponding to 24.22% improvement, while the OLDH-2 reveals a 10.56% increase. These good results are attributed to homogeneously dispersed filler, as clearly seen from the results given in previous sections. In particular, the well-dispersed fillers have created the tortuous paths, which have influenced the kinetics of water vapor diffusion, thereby resulting in decreased polymer permeability. Considering the excellent optical property of composite films, the results of this study have shown that there is a good potential in reducing film permeability using very low loading nanosized OLDH, which, in turn, maintains and even enhances film transparency.

Thermal stability

To explore the influence of OLDH on thermal properties of PVA films, the TGA and DTG curves of the OLDH powder, pure PVA film (OLDH-0) and PVA/OLDH films (OLDH-1, OLDH-2 and OLDH-4) are represented in Fig. 8. The mass loss of OLDH at three temperature ranges of 30–144, 144–234 and 234–600 °C are attributed, to the loss of surface-adsorbed water and interlayer water in OLDH, the decomposition of intercalated PDP and the collapse of the layered structure of OLDH phase, and the decomposition of residual carbon, as in the order given [36].

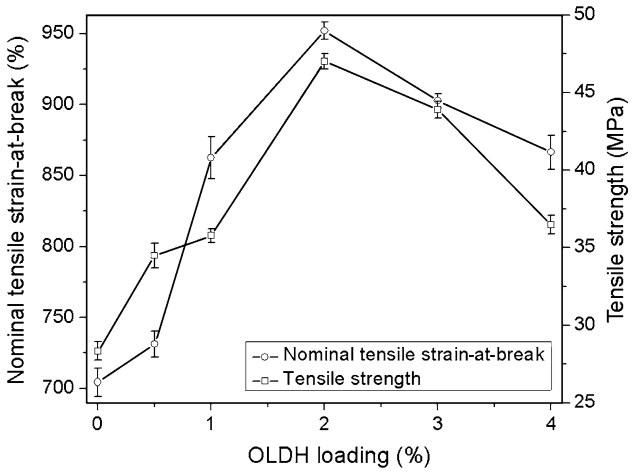

Fig. 6 Nominal tensile strain-at-break and tensile strength variations as functions of OLDH loading

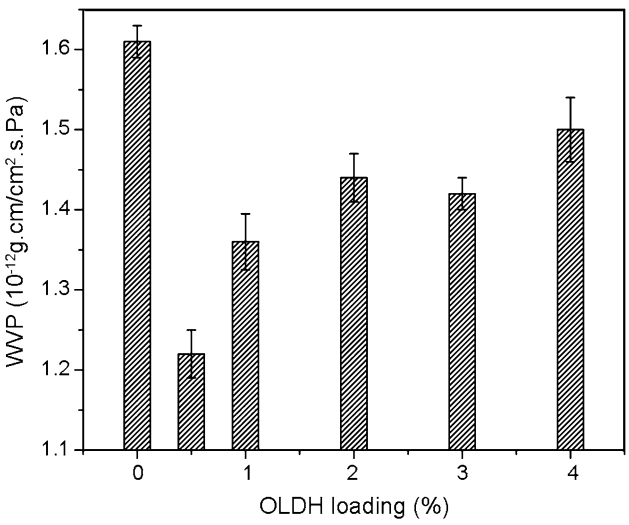

Fig. 7 Water vapor permeability variation as a function of OLDH loading

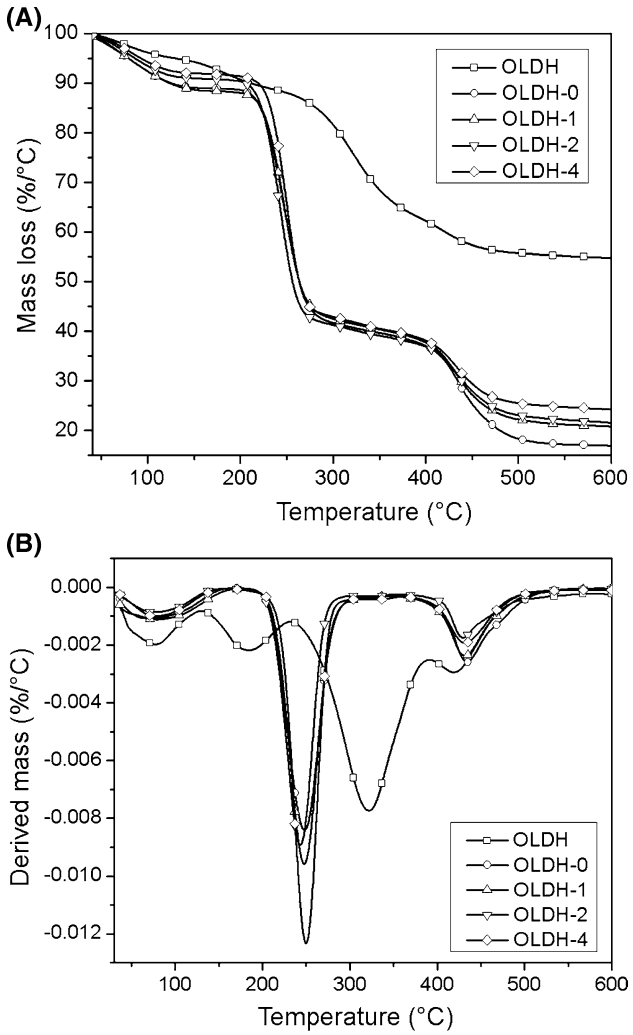

Fig. 8 **a** TGA and **b** DTG curves of OLDH powder and OLDH/PVA samples

The pure PVA and PVA/OLDH films show a three-stage degradation process based on DTG profiles corresponding to the release of absorbed water, degradation of PVA chains and the heat-rearrangement of the polyalkene structure to a polyaromatic form, and dehydration of the PVA chains [24]. The final residual amount of pure PVA was measured and found to be 16.94 wt%. It is observed that by the addition of nanosized OLDH the thermal stability is markedly enhanced. The decomposition rates of PVA/OLDH films are slower than those of pure PVA film in the first and third steps, while the second-step decomposition rate is more rapid in composite films. The reduced decomposition rate of the first step might be attributed to the strong interactions between the OLDH nanosheets and PVA matrix, and the physical barrier effect of the LDH nanosheets [37]. With temperature increase, the decomposition of the intercalated PDP occurs and the decomposition rate increases faster with OLDH (PDP) loading, as seen in Fig. 8b. It should be noted that, the decomposition rate at the third step is much slower in pure PVA film, therefore, the higher residual char contents are observed for composite films (OLDH-1: 20.85%, OLDH-2: 21.56%, OLDH-4: 24.20%).

As it is known, phosphorus is a flame retardant which can delay the decomposition process in solid state through formation of polymetaphosphate. The results indicate that the PDP-modified LDH sheets dispersed in a PVA matrix could provide a protective shield of mass and heat transfer, which could slow down the heat release rate and the effusion of decomposed small molecules through the polymer matrix. Comparing with the previous results associated with weaker thermal performance [38], the nanosized OLDH, presented in this work, seems to be capable of improving the thermal stability of PVA films. We considered the PVA/OLDH (2%) film as the optimal film composition with optimum optical property, mechanical performance, water vapor barrier property and thermal stability for use in packaging applications.

Conclusion

In this work, a series of biodegradable nanocomposite films based on PVA and OLDH with enhanced optical, mechanical, water vapor barrier and thermal stability properties were fabricated by solution casting method. Compared with a pure PVA film, the PVA/OLDH (2%) film showed an optimal optical property with improvement in haziness by 67% and the best mechanical performance by 66% enhancement in tensile strength. Furthermore, an improvement by 10.56% in water vapor barrier property was observed along with an enhanced thermal stability. The enhancement of overall performance could be attributed to an effective dispersion of PDP-intercalated OLDH in polymer matrix, and strong interactions between the nanosized OLDH nanosheets and PVA. Therefore, high performance of PVA/OLDH nanocomposite films makes them suitable in promoting their applications as biodegradable PVA films in packaging industry.

Acknowledgements This work was funded by the National Key Research and Development Program (Grant No. 2016YFB0302403), the Project of Shandong Province Education Department (Grant No. ZR2014JL023), the National Natural Science Foundation of China (Grant No. 31572201), the Natural Science Foundation of Shandong Province (Grant No. ZR2015CM035), Shandong Agricultural Innovation Team (Grant No. SDAIT-17-04), the Projects of Commercialization of Research Findings of Shandong Province (Grant No. [2014] 183), the Great Innovation Projects in Agriculture of Shandong Province (Grant No. [2013] 136), the National Natural Science Foundation of China (Grant No. 21375079), and Shandong Youth Education Science Program for College Students (Grant No. 17BSH113).

References

1. Achaby ME, Miri NE, Aboulkas A, Zahouily M, Bilal E, Barakat A, Solhy A (2017) Processing and properties of eco-friendly bionanocomposite films filled with cellulose nanocrystals from sugarcane bagasse. Int J Biol Macromol 96:340–352
2. Ayana B, Suin S, Khatua BB (2014) Highly exfoliated ecofriendly thermoplastic starch (TPS)/poly(lactic acid)(PLA)/clay nanocomposites using unmodified nanoclay. Carbohydr Polym 110:430–439
3. Youssef AM, Elsayed SM, Salama HH, Elsayed HS, Dufresne A (2015) Evaluation of bionanocomposites as packaging material on properties of soft white cheese during storage period. Carbohydr Polym 132:274–285
4. Xie J, Zhang K, Wu J, Ren G, Chen H, Xu J (2016) Bio-nanocomposite films reinforced with organo-modified layered double hydroxides: preparation, morphology and properties. Appl Clay Sci 126:72–80
5. Li GF, Luo WH, Xiao M, Wang SJ, Meng YZ (2016) Biodegradable poly(propylene carbonate)/layered double hydroxide composite films with enhanced gas barrier and mechanical properties. Chin J Polym Sci 34:13–22
6. Ahmed J, Mulla M, Arfat YA (2017) Application of high-pressure processing and polylactide/cinnamon oil packaging on chicken sample for inactivation and inhibition of *Listeria monocytogenes* and *Salmonella* Typhimurium, and post-processing film properties. Food Control 78:160–168
7. Singha AS, Kapoor H (2014) Effects of plasticizer/cross-linker on the mechanical and thermal properties of starch/PVA blends. Iran Polym J 23:655–662
8. Tripathi S, Mehrotra GK, Dutta PK (2010) Preparation and physicochemical evaluation of chitosan/poly(vinyl alcohol)/pectin ternary film for food-packaging applications. Carbohydr Polym 79:711–716
9. Sen C, Das M (2017) Self-supporting-film from starch, poly(vinyl alcohol), and glutaraldehyde: optimization of composition using response surface methodology. J Appl Polym Sci 134:44436–44447
10. Jiménez A, Arab-Tehrany E, Sánchez-González L (2014) Progress in biodegradable packaging materials. Prog Nanomater Food Packaging:50–65
11. Chaabouni O, Boufi S (2017) Cellulose nanofibrils/polyvinyl acetate nanocomposite adhesives with improved mechanical properties. Carbohydr Polym 156:64–70
12. Ma Q, Du L, Yang Y, Wang L (2017) Rheology of film-forming solutions and physical properties of tara gum film reinforced with polyvinyl alcohol (PVA). Food Hydrocoll 63:677–684
13. Jan R, Habib A, Akram MA, T-u-H Zia, Khan AN (2016) Uniaxial drawing of graphene-PVA nanocomposites: improvement in mechanical characteristics via strain-induced exfoliation of graphene. Nanoscale Res Lett 11:377–386
14. Sugumaran S, Bellan CS, Muthu D, Raja S, Bheeman D, Rajamani R (2015) New transparent PVA-InTiO hybrid thin films: influence of InTiO on the structure, morphology, optical, and dielectric properties. Polym Adv Technol 26:1486–1493
15. Zhou CH (2010) Emerging trends and challenges in synthetic clay-based materials and layered double hydroxides preface. Appl Clay Sci 48:1–4
16. Hennous M, Derriche Z, Privas E, Navard P, Verney V, Leroux F (2013) Lignosulfonate interleaved layered double hydroxide: a novel green organoclay for bio-related polymer. Appl Clay Sci 71:42–48
17. Yang ZZ, Wang FH, Zhang C, Zeng GM, Tan XF, Yu ZG, Zhong Y, Wang H, Cui F (2016) Utilization of LDH-based materials as potential adsorbents and photocatalysts for the decontamination of dyes wastewater: a review. RSC Adv 6:79415–79436
18. Wang LJ, Wang LR, Feng YJ, Feng JT, Li DQ (2011) Highly efficient and selective infrared absorption material based on layered double hydroxides for use in agricultural plastic film. Appl Clay Sci 53:592–597
19. Gao X, Hu M, Lei L, O'Hare D, Markland C, Sun Y, Faulkner S (2011) Enhanced luminescence of europium-doped layered double hydroxides intercalated by sensitiser anions. Chem Commun 47:2104–2106
20. Chen C, Byles C, Buffet JC, Rees N, Wu Y, Ohare D (2016) Core-shell zeolite@aqueous miscible organic-layered double hydroxides. Chem Sci 7:1457–1461
21. Ciou CY, Li SY, Wu TM (2014) Morphology and degradation behavior of poly(3-hydroxybutyrate-*co*-3-hydroxyvalerate)/layered double hydroxides composites. Eur Polym J 59:136–143
22. Liau CP, Bin Ahmad M, Shameli K, Yunus WMZW, Ibrahim NA, Zainuddin N, Then YY (2014) Preparation and characterization of polyhydroxybutyrate/polycaprolactone/Mg–Al layered double hydroxide nanocomposites. Dig J Nanomater Bios 9:71–82
23. Roy S, Srivastava SK, Pionteck J, Mittal V (2015) Assembly of layered double hydroxide on multi-walled carbon nanotubes as reinforcing hybrid nanofiller in thermoplastic polyurethane/nitrile butadiene rubber blends. Polym Int 65:93–101
24. Zhou K, Gui Z, Hu Y (2017) Facile synthesis of LDH nanoplates as reinforcing agents in PVA nanocomposites. Polym Adv Technol 28:386–392
25. Marangoni R, da Costa Gardolinski JEF, Mikowski A, Wypych F (2011) PVA nanocomposites reinforced with Zn_2Al LDHs, intercalated with orange dyes. J Solid State Electrochem 15:303–311
26. Xie JZ, Zhang K, Zhao QH, Wang QG, Xu J (2016) Large-scale fabrication of linear low density polyethylene/layered double hydroxides composite films with enhanced heat retention, thermal, mechanical, optical and water vapor barrier properties. J Solid State Chem 243:62–69
27. Zhao Y, Li F, Zhang R, Evans DG, Duan X (2002) Preparation of layered double-hydroxide nanomaterials with a uniform crystallite size using a new method involving separate nucleation and aging steps. Chem Mater 14:4286–4291
28. Quan ZL, Yang H, Zheng B, Hou WG (2009) Synthesis and release behavior of bactericides intercalated Mg–Al layered double hydroxides. Colloid Surface A 348:164–169
29. Chen W, Qu B (2003) Structural characteristics and thermal properties of PE-g-MA/MgAl-LDH exfoliation nanocomposites synthesized by solution intercalation. Chem Mater 15:3208–3213
30. Hiraide T, Kageyama H, Nakagawa Y, Oaki Y, Imai H (2016) UV-induced epitaxial attachment of TiO_2 nanocrystals in molecularly mediated 1D and 2D alignments. Chem Commun 52:7545–7548
31. Gao YS, Wu JW, Zhang Z, Jin R, Zhang X, Yan XR, Umar A, Guo ZH, Wang Q (2013) Synthesis of polypropylene/Mg_3Al-X (X = CO_3^{2-}, NO_3^-, Cl^-, SO_4^{2-}) LDH nanocomposites using a solvent mixing method: thermal and melt rheological properties. J Mater Chem A 1:9928–9934
32. Pak YL, Bin Ahmad M, Shameli K, Yunus WMZW, Ibrahim NA, Zainuddin N (2013) Preparation and characterization of poly-3-hydroxybutyrate/poly (butyleneadipate-coterephthalate)/layered double hydroxide nanocomposites. Dig J Nanomater Biostruct 8:1395–1403
33. Rad FA, Rezvani Z (2015) Preparation of cubane-1,4-dicarboxylate-Zn–Al layered double hydroxide nanohybrid: comparison of structural and optical properties between experimental and calculated results. RSC Adv 5:67384–67393
34. Mohanty S, Nayak SK (2012) Biodegradable nanocomposites of poly(butylene adipate-*co*-terephthalate) (PBAT) and organically modified layered silicates. J Polym Environ 20:195–207

35. Ramaraj B, Nayak SK, Yoon KR (2010) Poly(vinyl alcohol) and layered double hydroxide composites: thermal and mechanical properties. J Appl Polym Sci 116:1671–1677
36. Arizaga GGC, Wypych F, Barraza FC, Lopez OEC (2010) Reversible intercalation of ammonia molecules into a layered double hydroxide structure without exchanging nitrate counter-ions. J Solid State Chem 183:2324–2328
37. Matusinovic Z, Wilkie CA (2012) Fire retardancy and morphology of layered double hydroxide nanocomposites: a review. J Mater Chem 22:18701–18704
38. Ramaraj B, Jaisankar SN (2008) Thermal and morphological properties of poly(vinyl alcohol) and layered double hydroxide (LDH) nanocomposites. Polym Plast Technol Eng 47:733–738